

Reactions of Free Radicals Produced by Laser Photolysis

Louise Pasternack, H. H. Nelson,¹ and J. R. McDonald

Chemistry Division, Naval Research Laboratory, Washington, DC 20375

Mechanisms involving free radicals reacting rapidly are important in combustion chemistry, air pollution, and atmospheric chemistry. Yet, very little experimental data is available on radical reactions. They are difficult to study in situ. In a methane flame, for example, modelers predict that more than 30 different elementary reactions are important (1). What is needed is to isolate individual reactions.

There are three major difficulties in such studies:

- (1) We must first generate free radicals in large enough concentrations to carry out kinetic studies. Clean sources of these radicals must be available to minimize competing reactions.
- (2) Techniques for monitoring the free radicals must be available.
- (3) Since radical reactions can be very fast, techniques for studying kinetics over a wide range of time scales must be available. (In our experiments we measure reaction rates ranging from gas kinetic to five orders of magnitude slower than gas kinetic.)

In this paper we will present the general techniques we use and then show, using the examples of C₂ and C₃ reactions, how the techniques are employed and the kinds of information about fast free radical reactions that can be gained. Some recent review articles are available (2, 3) which are more comprehensive.

Although a number of techniques exist for creating free radicals, I will be discussing only the use of pulsed laser photolysis. This technique is particularly useful for several reasons.

- (1) It is a pulsed system so that initiation of the reaction can take place on a time scale that is short compared to the reaction time scale.
- (2) Monochromatic light allows formation of specific radicals which reduces the number of competing reactions.
- (3) The high spectral brightness of lasers improves the yield of radicals as compared to flashlamp techniques.
- (4) Since different lasers, some of which are tunable, can be used to attain different frequencies, the technique can produce many different radicals.

However, this technique is not universal. The reagent gas must be transparent to the photolysis frequency and the reactant must exhibit a laser-induced fluorescence signal.

In our laboratory, we have used UV excimer lasers and frequency quadrupled Nd:YAG lasers for photolysis. Excimer lasers have been described in more detail by W. F. Coleman in this symposium. A discharge through a mixture of a rare gas and halogen produces a rare gas halide in a bound upper state. This fluoresces to the ground state which dissociates, maintaining the population inversion to sustain lasing. We operate the laser on ArF at 193 nm and on KrF at 248.5 nm. The quadrupled Nd:YAG laser operates at 266 nm. In other laboratories, CO₂ lasers which operate in the infrared are used for photolysis. Some of the radicals produced by UV laser photolysis include C₂, C₃, CH, CH₂, C₂O, CH₃O (methoxy), CH₂CHO (vinoxy), C₆H₅CH₂ (benzyl), C₅H₅ (cyclopentadienyl), CN, OH, and O(¹D). We will discuss the specific photolysis processes used to form C₂ and C₃ later in this paper. In our laboratory, we have looked primarily at the reactions of these species with hydrocarbons and oxygen which might be of importance in combustion.

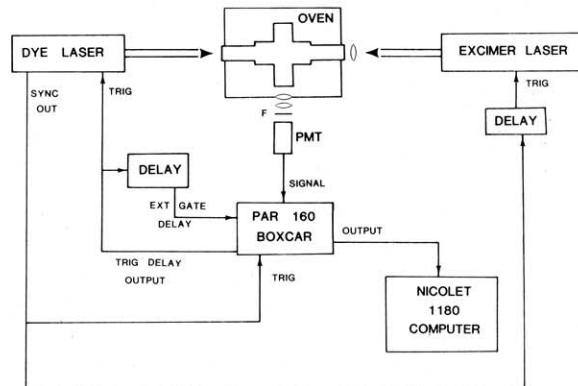


Figure 1. Multiphoton UV photolysis laser-laser fluorescence detection apparatus schematic.

Laser techniques used to monitor radicals include IR laser absorption, intracavity absorption, optoacoustic techniques, and laser-induced fluorescence. We used laser-induced fluorescence because of its sensitivity. It is limited in its applicability to molecules which fluoresce, which include the radicals that are listed above. D. R. Crosley has discussed laser-induced fluorescence (LIF) in detail in the previous paper. Essentially, a laser induces a resonant electronic transition from a particular vibrational level in the ground (or metastable) state to a particular vibrational level in an excited state. The molecule then fluoresces to the lower state, and it is this fluorescence that is measured. For these studies, we use a tunable dye laser (either a flashlamp pumped dye laser or a Nd:YAG pumped dye laser). This probe laser can be delayed in time with respect to the photolysis laser, allowing us to monitor the time evolution (disappearance rate) of the free radical. In most cases we do not monitor products so that in general we cannot sort complicated mechanisms. However, by structuring our experiments to look at isolated elementary reactions of free radicals, we can determine their reaction rates.

Experimental

The apparatus we used is shown in Figure 1. Experiments are performed in bulbs, not beams, because it is simpler and the apparatus is more flexible. We use a stainless steel cross with typically 2 mTorr of precursor, 20 mTorr–10 Torr of reactant and several torr of buffer gas for rotational, vibrational, and translational cooling. The gases are either mixed in the cross or premixed and slowly flowed through the cross to prevent product buildup. The cross is situated inside a mechanical convection oven for studies of reactions at higher than ambient temperatures.

Radicals are generated by a photodissociation process using a focused excimer laser. A tunable dye laser, collinear to the photolysis laser, is used to monitor the free radicals using LIF. The fluorescence is monitored at 90° using a photomultiplier, and the signal is averaged using a boxcar integrator. A computer is used to fit the data.

¹ NRC/NRL Research Associate.

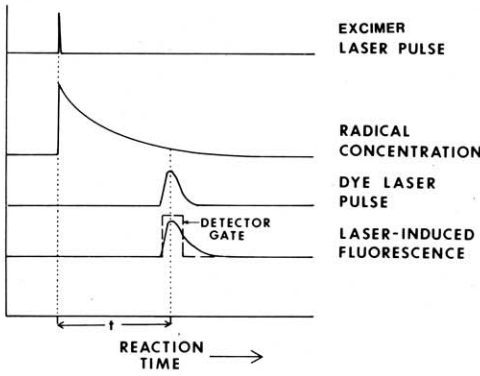


Figure 2. Timing sequence for monitoring disappearance rates.

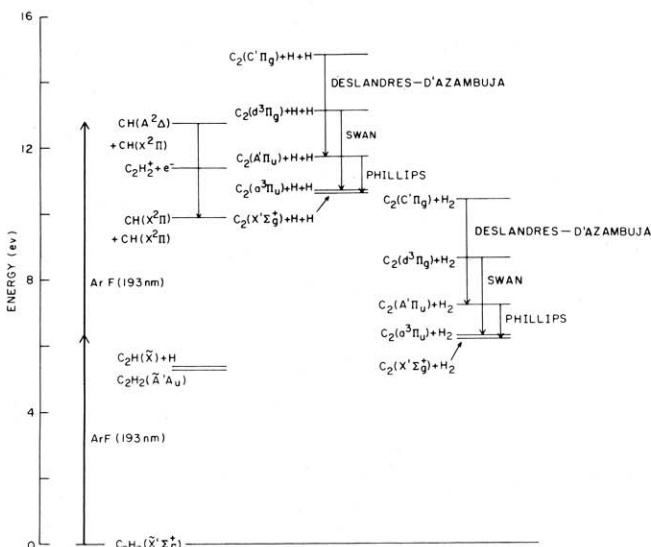


Figure 3. Energy level diagram for photochemical processes relevant to C_2H_2 multiphoton UV dissociation. From ref. 8.

The photolysis laser pulse initiates the reaction by forming the radicals. The timing sequence is shown in Figure 2. The radicals react and disappear over time (typically several hundred μs) The probe laser used to monitor the radical concentration is scanned in time after the photolysis.

The rate of depletion of the radical is monitored by varying the time between the photolysis and probe laser pulses. The process is automated by using the boxcar integrator gate to trigger the probe laser so that both can be synchronously scanned in time following the photolysis.

C₂ Experiments

The first set of experiments we consider as an example involve reactions of C_2 in its ground $\text{X}^1\Sigma_g^+$ state and metastable $\text{a}^3\Pi_u$ state with hydrogen and small hydrocarbons (4–6). These states are separated by 610 cm^{-1} (1.7 kcal/mole), thus providing an opportunity to study gas phase elementary reactions involving two nearly isoenergetic states differing in spin and electronic symmetry. In addition, C_2 is present in combustion systems; for example the concentration of ${}^3\text{C}_2$ in oxyacetylene flames is 0.1 Torr (7).² Clearly the reaction rates of a radical present at such high concentrations must be known before modeling of hydrocarbon fuels can be undertaken with confidence.

² ${}^1\text{C}_2$ and ${}^3\text{C}_2$ are used to denote the $\text{X}^1\Sigma_g^+$ and $\text{a}^3\Pi_u$ states of C_2 , respectively.

C_2 can be formed using UV laser photolysis of almost any unsaturated hydrocarbon. We used 193 nm photolysis of acetylene to form ${}^3\text{C}_2$ (4) and hexafluorobutene-2 to form ${}^1\text{C}_2$ (5). The photolysis scheme for acetylene (8) is shown in Figure 3. There are two possible channels for C_2 formation: (1) concerted molecular elimination of H_2 or (2) elimination of 2 H atoms. Both require at least two photons. The evidence favors H atom elimination for three reasons: (1) It is spin forbidden for singlet acetylene to photodissociate to ${}^3\text{C}_2$ and singlet H_2 . (2) We observe (8) a three-photon dependence of $\text{C}_2\text{d}^3\Pi_g$ formation which is consistent with the energetics of H atom elimination, and (3) we observe (8) $\text{C}_2\text{A}^1\Pi_u$ in vibrational levels up to $v = 5$ which is also consistent with the energetics of H atom elimination. If H_2 were formed, enough energy would be available to dissociate $\text{C}_2\text{A}^1\Pi_u$. Unfortunately, we cannot determine if the process is sequential, going by one photon absorption to form C_2H and a second photon absorption to form C_2 or whether the process is a direct, two photon absorption into acetylene.

The photodissociation of acetylene and hexafluorobutene-2 yield a variety of products, many of which are in electronically excited states resulting in prompt fluorescence. In order to see LIF from the ground state, this emission must be quenched using a buffer gas. In addition, the C_2 in the ground and metastable $\text{a}^3\Pi_u$ state are vibrationally and rotationally hot. Since we monitor only the lowest vibrational level using LIF, we must either (a) completely thermalize the vibrational distribution in $20 \mu\text{s}$, or (b) not relax upper levels into $v'' = 0$ in the $\approx 300 \mu\text{s}$ it takes for the reaction. CH_4 quickly vibrationally thermalizes the ${}^3\text{C}_2$ so we use it as a buffer. However, CH_4 reacts with ${}^1\text{C}_2$, so instead we use He as a buffer in the ${}^1\text{C}_2$ experiments since it does not vibrationally quench the ${}^1\text{C}_2$ over the reaction time scale.

LIF is used to probe the C_2 concentrations. $\text{C}_2\text{X}^1\Sigma_g^+$ populations are probed by exciting the $\text{A}^1\Pi_u v' = 4 \leftarrow \text{X}^1\Sigma_g^+ v'' = 0$ Phillips band transition at 691 nm and detecting $4 \rightarrow 1$ fluorescence at 792 nm. $\text{C}_2\text{a}^3\Pi_u$ populations are probed by exciting the 0–0 band of the $\text{a}^3\Pi_u \rightarrow \text{d}^3\Pi_g$ Swan band at 516.5 nm and observing LIF on the 0–1 vibronic band at 563 nm. These are both done with a CMX-4 flashlamp pumped dye laser.

By monitoring the disappearance of ${}^3\text{C}_2$ over time in the presence of hydrogen and small hydrocarbons, we believe we are monitoring the rate of reaction of ${}^3\text{C}_2$ and not quenching to the ground state. It is spin forbidden for ${}^3\text{C}_2$ to be quenched by a singlet hydrocarbon. Resonant spin exchange is not possible since the energy spacing between triplet and singlet C_2 is only 610 cm^{-1} and spin orbit coupling is generally weak for hydrogen and small hydrocarbons.

The kinetics of the reaction can be expressed by

$$\frac{d[\text{C}_2]}{dt} = -k_{II}[\text{C}_2][\text{Reactant}] - k_p[\text{C}_2][\text{precursor}]$$

in the absence of diffusion. We perform these experiments under pseudo-first-order conditions where the concentration of reactant is much larger than the concentration of C_2 . Under these conditions,

$$\frac{d[\text{C}_2]}{dt} \simeq -k_1[\text{C}_2]$$

We can solve this equation:

$$[\text{C}_2] = [\text{C}_2]_0 \exp(-k_1 t)$$

where $k_1 = k_{II}[\text{reactant}] = k_p[\text{precursor}]$. Thus, a plot of $\log [\text{C}_2]$ versus t gives a straight line with slope k_1 and a plot of k_1 versus reactant pressure gives a line with slope k_{II} and an intercept proportional to the rate of reaction of C_2 with the precursor. In Figure 4 a typical first order decay is shown. The decay is linear over 4 reaction lifetimes. The risetime is an experimental artifact resulting from the overlap of the short

excimer pulse with the long tail of the dye laser, broadened by the boxcar integrator. Figure 5 shows a plot of k_1 versus reactant pressure for the $\text{C}_2 + \text{C}_2\text{H}_2$ reaction. These experiments were performed using different buffer gases at different pressures to be sure that there are no effects due to vibrational relaxation, diffusion, or three-body reactions. More typical data for several reactions of ${}^1\text{C}_2$ are shown in Figure 6.

In Table 1, the bimolecular rate constants for $\text{C}_2\text{X}^1\Sigma_g^+$ and a ${}^3\Pi_u$ reactions are listed. $\text{C}_2\text{X}^1\Sigma_g^+$ reacts considerably faster than $\text{C}_2\text{a}^3\Pi_u$ with hydrogen and hydrocarbons, especially H_2 and CH_4 where the difference may be more than 5 orders of magnitude at room temperature. Since both triplet and singlet C_2 reactions are spin allowed to form $\text{C}_2\text{H} + \text{H}$ and are nearly isoenergetic, the difference in reaction rate must be due to a difference in mechanism due to the different electronic states.

Although it appears that the reaction of C_2 with O_2 is the same for ${}^1\text{C}_2$ and ${}^3\text{C}_2$, Mangir et al. (9) have shown that what we are seeing is the reaction of equilibrated triplets and singlets. The quenching of ${}^3\text{C}_2$ by O_2 is spin allowed and it turns out that it is more than an order of magnitude faster than reaction.

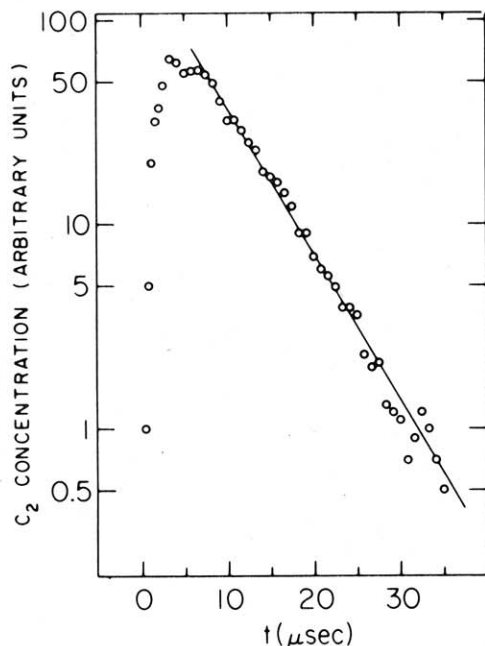


Figure 4. A plot of the $\text{C}_2\text{a}^3\Pi_u$ pseudo-first-order decay in the presence of excess C_2H_2 . $P_{\text{C}_2\text{H}_2} = 48.8$ mTorr, $P_{\text{N}_2} = 9.8$ Torr; $k_1 = 0.141 \mu\text{sec}^{-1}$. From ref. 4.

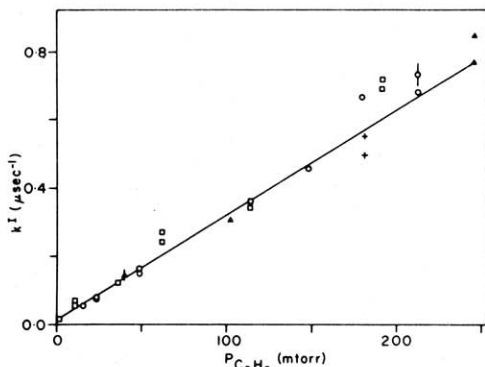


Figure 5. A plot of k_1 versus $P_{\text{C}_2\text{H}_2}$ for the reaction of $\text{C}_2\text{a}^3\Pi_u$ with C_2H_2 . A linear least squares fit of the data gives a slope corresponding to a second order rate constant, $k_{11} = (9.6 \pm 0.3) \times 10^{-11} \text{ cm}^3 \text{ molecule}^{-1} \text{ sec}^{-1}$. Symbols represent Ar (Δ), N_2 (O), CH_4 (□) and SF_6 (+) buffer gases. From ref. 4.

Reisler, et al. (10) have also measured the rate constants for reactions of ${}^1\text{C}_2$ and ${}^3\text{C}_2$. Where there is overlap with our experiments (for H_2 , CH_4 , and O_2 reactions) the values are in agreement with the exception of C_3H_8 reactions. For the reaction of C_3H_8 with ${}^3\text{C}_2$, we obtained a room temperature rate constant of $(1.35 \pm 0.04) \times 10^{-11} \text{ cm}^3 \text{ molecule}^{-1} \text{ sec}^{-1}$ (6) as compared to the value of $(1.66 \pm 0.10) \times 10^{-10} \text{ cm}^3 \text{ molecule}^{-1} \text{ sec}^{-1}$ obtained by Reisler, et al. (10). We have carefully checked our propane measurements and can find no way to rationalize our results with those of Reisler, et al.

There are two possible mechanisms for these reactions: hydrogen abstraction or insertion. Based on molecular orbital considerations discussed later, ${}^3\text{C}_2$ can react only by addition, but ${}^1\text{C}_2$ can react also by insertion. This is consistent with O atom (11-12) and CH_2 (13-15) reactions with hydrogen and small hydrocarbons where it has been determined that the singlet state reacts by insertion and addition and the triplet state reacts only by abstraction.

To test this, we measured the activation energies of these reactions by measuring their temperature dependence. The bimolecular rate constants are then fit to the Arrhenius equation $k_{11}(T) = A \exp(-E_a/RT)$. The Arrhenius plots for

Table 1. Rate constants ($\text{cm}^3 \text{ s}^{-1} \text{ molecule}^{-1}$) for the disappearance of $\text{C}_2\text{X}^1\Sigma_g^+$ compared to $\text{C}_2\text{a}^3\Pi_u$ at 298 K (1 σ uncertainty)

Reactant	$k_{11}(\text{C}_2\text{X}^1\Sigma_g^+)^a$	$k_{11}(\text{C}_2\text{a}^3\Pi_u)$
H_2	$(1.38 \pm 0.06) \times 10^{-12}$	$(6.0 \pm 1.5) \times 10^{-16}^b$
CH_4	$(1.87 \pm 0.05) \times 10^{-11}$	$(1.4 \pm 0.4) \times 10^{-15}^b$
C_2H_2	—	$(9.6 \pm 0.3) \times 10^{-11}^c$
C_2H_4	$(3.26 \pm 0.05) \times 10^{-10}$	$(1.44 \pm 0.06) \times 10^{-10}^c$
C_2H_6	$(1.59 \pm 0.05) \times 10^{-10}$	$(1.21 \pm 0.02) \times 10^{-12}^d$
C_3H_8	—	$(1.35 \pm 0.04) \times 10^{-11}^d$
$n\text{-C}_4\text{H}_{10}$	—	$(4.1 \pm 0.2) \times 10^{-11}^d$
O_2	$(2.9 \pm 0.1) \times 10^{-12}^e$	$(2.9 \pm 0.1) \times 10^{-12}^e$
CO_2	—	no apparent reaction

^a From ref. 5.

^b From ref. 6, extrapolated to 298 K.

^c From ref. 4.

^d From ref. 6.

^e Value for the rate constant for the reaction of equilibrated ${}^1\text{C}_2$ and ${}^3\text{C}_2$. See text.

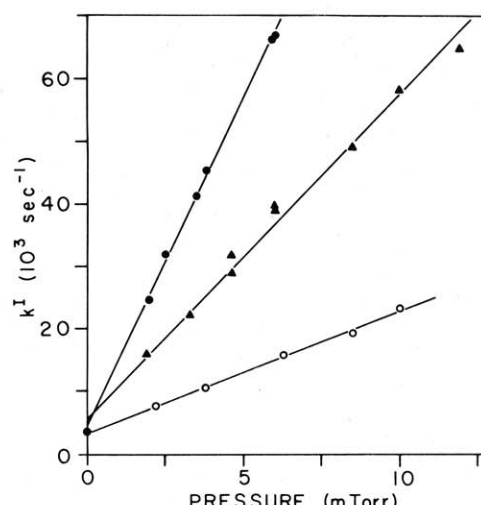


Figure 6. A plot of k_1 versus pressure for the reaction of $\text{C}_2\text{X}^1\Sigma_g^+$ with C_2F_4 (O), C_2H_6 (Δ), and C_2H_4 (●) using 2.2 mTorr of $\text{CF}_3\text{C}_2\text{CF}_3$ as a precursor for C_2 and He buffer gas ($P_{\text{He}} = 15$ Torr). The bimolecular rate constants, obtained from the slopes of the linear least-squares fits are $k_{11}(\text{C}_2\text{F}_4) = (5.99 \pm 0.14) \times 10^{-11} \text{ cm}^3 \text{ sec}^{-1} \text{ molecule}^{-1}$, $k_{11}(\text{C}_2\text{H}_6) = (1.59 \pm 0.05) \times 10^{-10} \text{ cm}^3 \text{ sec}^{-1} \text{ molecule}^{-1}$ and $k_{11}(\text{C}_2\text{H}_4) = (3.26 \pm 0.05) \times 10^{-10} \text{ cm}^3 \text{ sec}^{-1} \text{ molecule}^{-1}$. The intercepts correspond to the first order rate constant for $\text{C}_2 + \text{precursor}$. From ref. 5.

the reactions of $^3\text{C}_2$ are shown in Figures 7 and 8. The activation energies and preexponential factors are listed in Table 2.

The evidence for abstraction mechanism for $^3\text{C}_2 + \text{hydrogen}$ and small hydrocarbons comes from comparing our results using bond energy-bond order theory, linear free energy correlations, Evans-Polanyi plots and molecular orbital considerations.

Bond Energy-Bond Order Theory

The bond energy-bond order (BEBO) method (16-18) has been used to predict activation energies of numerous hydrogen abstraction reactions. It assumes a linear pseudotriatomic transition state $\text{R}-\text{H}-\text{C}_2$. The details of this calculation have been presented in reference 6. The values of the activation energy predicted by this technique are qualitatively similar to our experimental results but are too high by 2-4 kcal/mole. This may result from the approximations inherent in the BEBO theory: in particular, approximating a linear pseudotriatomic transition state and ignoring the contributions from the double bond to the bond order of the C—H bond.

Linear Free Energy Correlations

The other evidence for an abstraction mechanism for $^3\text{C}_2 + \text{RX}$ reactions is stronger. Linear, free energy correlations (19) provide support for this mechanism. Plots of $\log k$ (O^3P) and OH versus $\log k(^3\text{C}_2)$ are linear, as expected for reactions proceeding by the same mechanism. (See Fig. 9.) Values for the reaction with C_2H_4 do not lie on the lines, as might be expected since the double bond in ethylene makes reaction by insertion or addition more likely.

Evans-Polanyi Plot

Additional support is provided for the hydrogen abstraction mechanism from an Evans Polanyi plot of E_a versus energy required to remove H from $\text{R}-\text{H}$. Evans and Polanyi (20), in 1938, predicted that for hydrogen abstraction reactions, $E_a = \alpha[D_e(\text{C}-\text{H}) - c]$ where α and c are constants and $D_e(\text{C}-\text{H})$ is the dissociation energy for the carbon-hydrogen bond. (The dissociation energy of the C—H bond is weighted for the number of secondary and tertiary hydrogens since our experiments do not distinguish between them.) As predicted, we observe a linear relationship between the activation energy and the dissociation energy of the C—H bond (See Fig. 10.)

Molecular Orbital Considerations

We will only consider here the simplest reaction for molecular orbital considerations; $\text{C}_2 + \text{H}_2$. We will show that although abstraction reactions are allowed for triplet and singlet C_2 , insertion reactions are allowed only for $^1\text{C}_2$. This can account for the greater reactivity of $^1\text{C}_2$.

$^1\text{C}_2$ has the electronic configuration π^4 . The addition of a hydrogen 1s electron to a σ bonding orbital correlates with the ground state of C_2H which has the orbital configuration $\pi^4\sigma$. In contrast, $^3\text{C}_2$ has the electronic configuration $\pi^3\sigma$. In order for $^3\text{C}_2$ to react to form ground state C_2H , the H 1s electron would have to transfer to an orbital of π symmetry with respect to the long axis of the linear C_2H molecule, which is

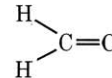
Table 2. Activation Energies and Preexponential Factors for Reactions of $^3\text{C}_2$

Reactant	E_a (kcal/mole)	$A(\text{cm}^3 \text{molecule}^{-1} \text{s}^{-1})$
H_2	5.99 ± 0.06	$(1.55 \pm 0.10) \times 10^{-11}$
D_2	7.37 ± 0.15	$(1.80 \pm 0.22) \times 10^{-11}$
CH_4^a	5.57 ± 0.11	$(1.65 \pm 0.20) \times 10^{-11}$
C_2H_6	1.83 ± 0.03	$(2.42 \pm 0.10) \times 10^{-11}$
C_3H_8	0.19 ± 0.07	$(1.84 \pm 0.17) \times 10^{-11}$
$n\text{-C}_4\text{H}_{10}$	0.14 ± 0.07	$(4.9 \pm 0.5) \times 10^{-11}$
C_2H_4	0.01 ± 0.09	$(1.20 \pm 0.16) \times 10^{-10}$

^a Pasternack, I., Baronavski, A. P., and McDonald, J. R., *J. Chem. Phys.*, **73**, 3508 (1980).

forbidden for linear approach. However, the H 1s electron could transfer to the σ bonding orbital, forming C_2H in the A^2II state which has the orbital configuration $\pi^3\sigma^2$. This is also an exothermic pathway. Thus, both $^1\text{C}_2$ and $^3\text{C}_2$ can react via an abstraction mechanism to form C_2H .

Reisler, Mangir, and Wittig (10) have drawn correlation diagrams for the insertion reactions of $\text{C}_2 + \text{H}_2$ which have high barriers for $^3\text{C}_2 + \text{H}_2$ reactions but low or no barriers for $^1\text{C}_2 + \text{H}_2$ reactions. For the case where reaction proceeds by broadside attack to form a



intermediate (see Fig. 11), they predict a 20 eV activation energy for hydrogen reactions with $^3\text{C}_2$. However, since $^1\text{C}_2$ has no electrons in the $p\sigma$ orbital, there is no significant barrier for $^1\text{C}_2 + \text{H}_2$ reactions. Similarly, for four center approach to form a bent acetylenic intermediate, a large barrier exists for $^3\text{C}_2 + \text{H}_2$ reactions, but $^1\text{C}_2 + \text{H}_2$ insertion reactions have no barrier (see Fig. 12).

What these experimental and molecular orbital considerations show, then, is that $^3\text{C}_2 + \text{H}_2$ can proceed *only* by abstraction whereas $^1\text{C}_2 + \text{H}_2$ can proceed also by insertion.

We have also determined experimental activation energies for $^1\text{C}_2$ reactions with H_2 and CH_4 (21) and found small but finite barriers of 2.9 kcal/mole for hydrogen and 0.6 kcal/mole for methane reactions. More accurate *ab initio* calculations are required to determine whether these can be predicted from an insertion mechanism.

C_3 Reactions

Another series of radical reactions we have studied using this technique is C_3 with saturated and unsaturated hydrocarbons (23). C_3 is observed in flames generally under fuel rich conditions of incipient soot formation. Under these conditions, as much as ~ 0.01 Torr of C_3 is present in the flame (22). We produced C_3 using 249 nm photolysis of benzene, (KrF laser).

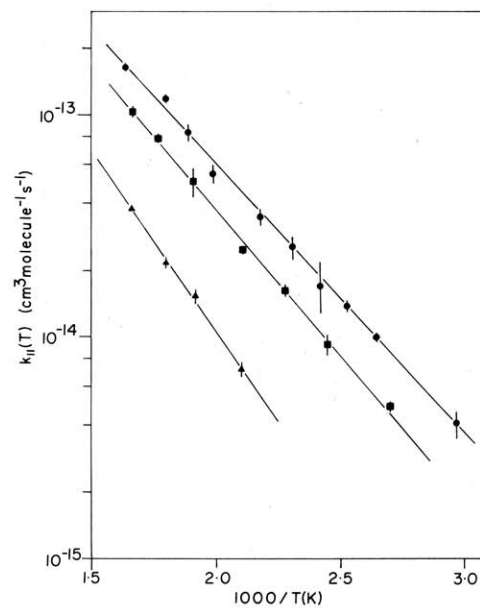


Figure 7. The Arrhenius plot of $\log k_{\text{II}}$ versus $1000/T$ for the reactions of $^3\text{C}_2$ with H_2 , D_2 , and CH_4 . The lines represent linear least squares fits to the data. The vertical error bars denote $\pm 2\sigma$. (\blacksquare) H_2 reaction: $E_a = 5.99 \pm 0.06$ kcal/mole, $A = (1.55 \pm 0.10) \times 10^{-11} \text{ cm}^3 \text{molecule}^{-1} \text{sec}^{-1}$; (\blacktriangle) D_2 reaction: $E_a = 7.37 \pm 0.15$ kcal/mole, $A = (1.80 \pm 0.22) \times 10^{-11} \text{ cm}^3 \text{molecule}^{-1} \text{sec}^{-1}$; (\bullet) CH_4 reaction: $E_a = 5.57 \pm 0.11$ kcal/mole, $A = (1.65 \pm 0.20) \times 10^{-11} \text{ cm}^3 \text{molecule}^{-1} \text{sec}^{-1}$. The error limits represent 1σ . From ref. 6.

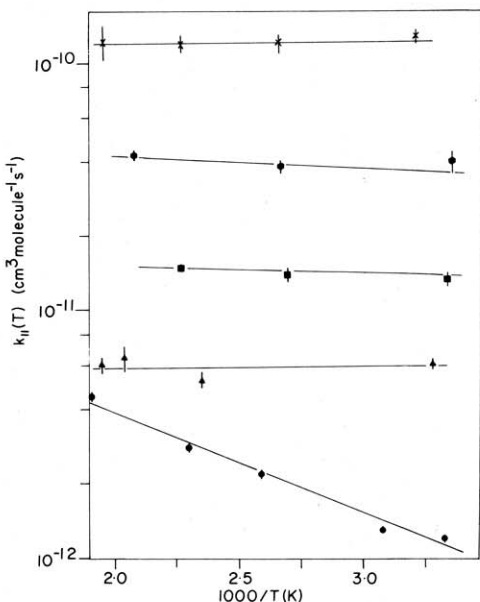


Figure 8. The Arrhenius plot of $\log k_{II}$ versus $1000/T$ for the reactions of ${}^3\text{C}_2$ with C_2H_6 (●); C_3H_8 (■); $n\text{-C}_4\text{H}_{10}$ (●); C_2H_4 (X); and the intersystem crossing of ${}^3\text{C}_2 \rightarrow {}^1\text{C}_2$ due to collisions with Xe (▲). From ref. 6.

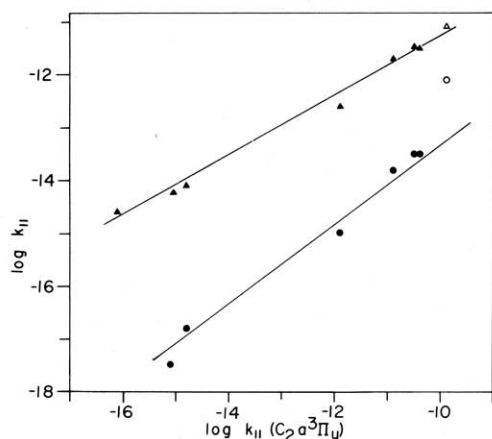


Figure 9. Linear free energy correlation of the rate coefficients for ${}^3\text{C}_2$ reactions with O^3P (●) and OH (▲) reactions which are known to proceed via hydrogen abstraction. The open symbols represent the rate coefficient for C_2H_4 reactions, which we postulate proceed by a different mechanism. From ref. 6.

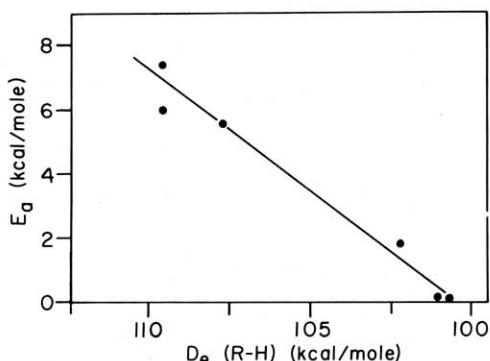


Figure 10. Evans-Polanyi plot of the activation energy versus the dissociation energy of the R—H bond. From ref. 6.

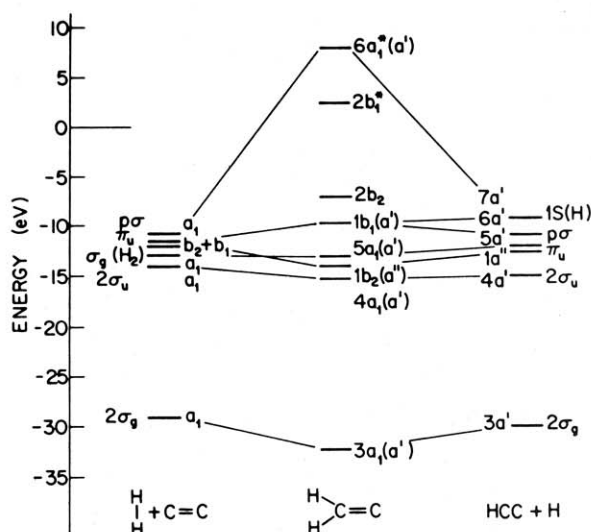


Figure 11. Molecular orbital correlation diagram for broadside $\text{C}_2 + \text{H}_2$. It is assumed that C_{2v} symmetry is maintained in the entrance channel. With ${}^1\text{C}_2$, four electrons are in π orbitals and the $2p\sigma$ orbital is vacant. With ${}^3\text{C}_2$, three electrons are in π_u orbitals and one is in a $2p\sigma$ orbital. A barrier in the entrance channel to the transition complex is evident with ${}^3\text{C}_2$. From ref. 10.

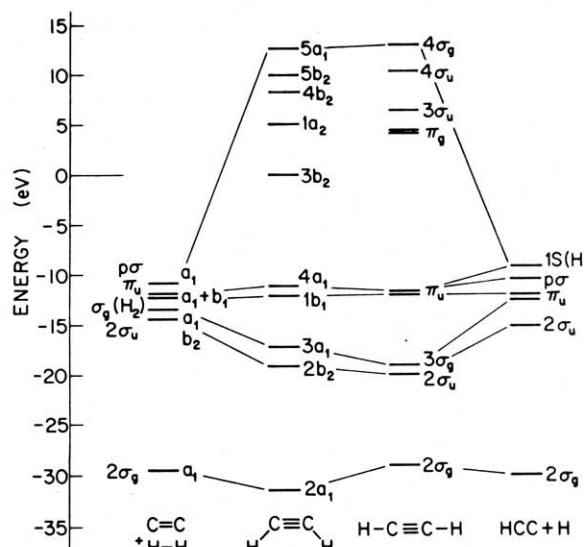


Figure 12. Molecular orbital correlation diagram for the four-center addition of H_2 to C_2 to form bent acetylene in the transition state. It is assumed that C_{2v} symmetry is maintained in the entrance channel. A barrier in the entrance channel to the transition complex is clearly evident in the ${}^3\text{C}_2 + \text{H}_2$ reaction. The electronic configuration of ${}^1\text{C}_2$ and ${}^3\text{C}_2$ are the same as in Figure 11. From ref. 10.

We measured C_3 laser-induced fluorescence by exciting the $\text{X}^1\Sigma_g^+ \rightarrow \text{A}^1\Pi$ 000–000 transition at 405 nm and monitoring fluorescence to the 000–002 level at 485 nm. A frequency doubled Nd:YAG laser operated in the sum mode with rhodamine 640 is used to obtain the probe frequency.

First-order rate constants were measured using similar techniques as for the C_2 reactions. An excess of reactant provides pseudo-first-order conditions. These reactions are performed by premixing the gases and slowly flowing them through the reaction cell to prevent build up of sooty products. The slope of a plot of first-order rate coefficients versus pressure gives the second-order rate constants. Some typical data is shown in Figure 13.

The second-order rate constants we obtained are listed in Table 3. The reaction of C_3 with alkanes is slower than $10^{-15} \text{ cm}^3 \text{ molecule}^{-1} \text{ sec}^{-1}$. The measured rates of reactions with alkenes vary from 10^{-15} to $10^{-11} \text{ cm}^3 \text{ molecule}^{-1} \text{ sec}^{-1}$, depending on the number of substituents on the double bond. Similarly, the rates of the alkyne reactions vary from $<10^{-15}$ to $10^{-11} \text{ cm}^3 \text{ molecule}^{-1} \text{ sec}^{-1}$ and the rates of the allenes vary from 10^{-13} to $5.2 \times 10^{-12} \text{ cm}^3 \text{ molecule}^{-1} \text{ sec}^{-1}$.

These observations are consistent with a mechanism involving electrophilic attack of the C_3 on the olefin π bond. This forms an intermediate containing cyclopropane. (See Fig. 14). Methyl substituents are electron donating and hence increase reactivity. Alkynes and allenes are probably more reactive because of the sizes and shapes of their π orbitals. Alkanes are less reactive for the same reason. Once the intermediate is formed, it may be stabilized by collision, or it could proceed to fall apart along the lines shown in Figure 14. Another possible fragmentation process would involve intramolecular rearrangement to form a ring compound. Product analysis by Skell and co-workers (24) of reactions of C_3 with unsaturated hydrocarbons performed by co-condensing C_3 and olefins on liquid N_2 surfaces is also consistent with a mechanism involving electrophilic attack to form molecules containing cyclopropane.

We have also looked at the reaction of C_3 with oxygen. It is slow; we see no reaction (i.e., $k_{II} < 10^{-15} \text{ cm}^3 \text{ molecule}^{-1} \text{ sec}^{-1}$). Thus, the major reaction that C_3 is likely to undergo

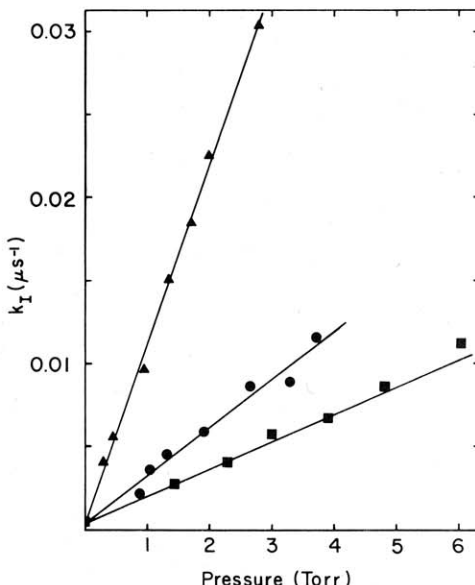


Figure 13. Plot of k_I versus pressure for the reaction of C_3 with (■) propene, (●) allene, and (▲) methylacetylene. Benzene was used as the precursor for the C_3 radical formation at 2 mTorr pressure. A total pressure of 20 Torr was maintained using N_2 as a buffer gas. From ref. 23.

Table 3. Rate Coefficients for the Disappearance of C_3 at 294 K ^a

Reactant	Structure	Reactant pressure (Torr)	$k_{II}(10^{-13} \text{ cm}^3 \text{ molecule}^{-1} \text{ s}^{-1})$ (1σ uncertainty)
I. Alkenes			
ethylene		0-68	<0.01
propene		0- 6.0	0.504 ± 0.031
1-butene		0- 4.8	0.917 ± 0.061
cis-2-butene		0- 0.98	4.16 ± 0.14
iso-butene		0- 0.082	48.3 ± 1.9
2-methyl-2-butene		0- 0.044	149 ± 10
II. Alkynes			
acetylene		0-50	<0.01
methylacetylene		0- 2.8	3.29 ± 0.07
1-pentyne		0- 0.48	5.59 ± 0.31
2-hexyne		0- 0.10	66.6 ± 3.0
III. Allenes			
allene		0- 3.71	0.89 ± 0.06
2,3-pentadiene		0- 0.40	10.7 ± 0.9
2,4-dimethyl-2,3-pentadiene		0- 0.07	52.3 ± 15.7

^a From ref. (23).

in combustion is with olefins to form larger carbon-rich, hydrogen-poor species.

Summary

These are only two of the many radical reactions that have been studied both in our laboratory and elsewhere using these techniques. Although the method is not universal, it does provide a means of studying many individual elementary reactions of free radicals. The two examples of C_2 and C_3 reactions presented in this paper demonstrate why these reactions are important as well as how the techniques can be applied and the information that can be obtained.

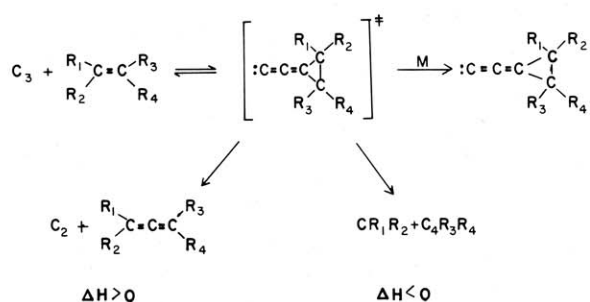


Figure 14. Possible mechanistic pathways for the reaction of C_3 with olefins.

Literature Cited

- (1) Olson, D. B., Gardiner, Jr., W. C., *J. Phys. Chem.*, **81**, 2514 (1977).
- (2) Lin, M. C. and McDonald, J. R., "Reactive Intermediates in the Gas Phase: Generation and Monitoring," D. W. Setser, (Editor), Academic Press, N. Y., 1979, pp. 223-304.
- (3) Reisler, H., Mangir, M., and Wittig, C., "Chemical and Biochemical Applications of Lasers," C. Bradley Moore, (Editor), Academic Press, New York, 1980, v. 5, pp. 139-174.
- (4) Donnelly, V. M. and Pasternack, L., *Chem. Phys.*, **39**, 427 (1979).
- (5) Pasternack, L. and McDonald, J. R., *Chem. Phys.*, **43**, 173 (1979).
- (6) Pasternack, L., Pitts, W. M., and McDonald, J. R., *Chem. Phys.*, **57**, 19 (1981).
- (7) Baronavski, A. P. and McDonald, J. R., *J. Chem. Phys.*, **66**, 3300 (1977); *Appl. Optics*, **16**, 1897 (1977).
- (8) McDonald, J. R., Baronavski, A. P., and Donnelly, V. M., *Chem. Phys.*, **33**, 161 (1978).
- (9) Mangir, M. S., Reisler, H., and Wittig, C., *J. Chem. Phys.*, **73**, 829 (1980).
- (10) Reisler, H., Mangir, M. S., and Wittig, C., *J. Chem. Phys.*, **73**, 2280 (1980).
- (11) Huie, R. E. and Herron, J. T., *Progr. Reaction Kinetics*, **8**, 1 (1975).
- (12) Bader, R. F. and Gangi, R. A., *J. Amer. Chem. Soc.*, **93**, 1831 (1971).
- (13) Braun, W., Bass, A. M., and Pilling, M., *J. Chem. Phys.*, **52**, 5131 (1970).
- (14) Bauschlicher, C. W., Schaefer, III, H. F., and Bender, C. F., *J. Amer. Chem. Soc.*, **98**, 1653 (1976); Bauschlicher, C. W., Bender, C. F., and Schaefer, III, H. F., *J. Amer. Chem. Soc.*, **98**, 3072 (1976); Bauschlicher, C. W., Haber, K., Schaefer, III, H. F., and Bender, C. F., *J. Amer. Chem. Soc.*, **99**, 3610 (1977).
- (15) Carr, Jr., R. W., *J. Phys. Chem.*, **76**, 1581 (1972).
- (16) Johnston, H. S., "Gas Phase Reaction Rate Theory," Ronald Press, N. Y., 1966.
- (17) Johnston, H. S. and Parr, C., *J. Amer. Chem. Soc.*, **85**, 2544 (1963).
- (18) Gilliom, R. D., *J. Chem. Phys.*, **65**, 5027, (1976).
- (19) Gaffney, J. S. and Levine, S. Z., *Intern. J. Chem. Kinetics*, **11**, 1197 (1979).
- (20) Evans, M. G. and Polanyi, M., *Trans. Faraday Soc.*, **34**, 11 (1938).
- (21) Pitts, W. M., Pasternack, L., and McDonald, J. R., *Chem. Phys.*, in press.
- (22) Gaydon, A. G., "The Spectroscopy of Flames," 2nd Ed., John Wiley and Sons, N. Y., 1974.
- (23) Nelson, H. H., Pasternack, L., Eyler, J. R., and McDonald, J. R., *Chem. Phys.*, **60**, 231 (1981).
- (24) Skell, P. S., Havel, J. J., and McGlinchey, M. J., *Accts. Chem. Res.*, **6**, 97 (1972).